JOURNAL OF THERMOPHYSICS AND HEAT TRANSFER
Vol. 12, No. 1, January–March 1998

Unidirectional Infiltration and Solidification/Remelting of Al–Cu Alloy

Jamil A. Khan* and Xinglin Tong†
University of South Carolina, Columbia, South Carolina 29208

Unidirectional, adiabatic infiltration, and solidification/remelting of Al-4.5 wt% Cu alloy in a porous preform is modeled numerically. The model formulation is derived from the fundamental conservation laws. The moving infiltration and remelting fronts are dealt with by the Landau transformation. The transformed governing equations are solved numerically. The solute, temperature, and solid volume fraction profiles are presented for representative parameters. The numerical predictions agree well with previously reported experimental measurements and with the analytical similarity solution. It is observed that the unidirectional infiltration and heat transfer do display the similarity behavior, and the macrosegregation in the casting is strongly dependent on the initial preform temperature, the superheat of inlet metal–matrix, and the applied pressure.

Nomenclature

C = solute concentration
c_p = specific heat at constant pressure
g_s = solid volume fraction
J = Jacobian of mapping
K = preform permeability
k_c = thermal conductivity of composite
k_p = partition coefficient
L = mold length
M = dimensionless remelting front position
m_1 = liquidus slope
Pr = Prandtl number
P_1 = inlet pressure
P_0 = outlet pressure
Ste = Stefan number
T_m = melting temperature of solvent
T_p = initial preform temperature
T_1 = inlet temperature
T_0 = liquidus temperature
t = time
U = dimensionless seepage velocity
u = seepage velocity
X = dimensionless coordinate
x = coordinate
Δh = latent heat of solidification
θ = dimensionless temperature
μ = dynamic viscosity
ν = kinematic viscosity
ξ = transformed coordinate
ρ = density
σ = ratio of thermal capacity
τ = dimensionless time
ς = preform porosity
Ψ = dimensionless pressure difference

Subscripts
av = average
c = composite
m = metal matrix
p = preform
1 = inlet

Received March 14, 1997; revision received July 16, 1997; accepted for publication July 17, 1997.

*Associate Professor, Department of Mechanical Engineering. E-mail: Jamil.khan@sc.edu.

†Graduate Research Assistant, Department of Mechanical Engineering, currently Graduate Student, Department of Mechanical Engineering, University of Iowa, Iowa City, IA 52246.

Introduction

COMPARED to the solid-state fabricating methods, such as powder metallurgy and foil diffusion bonding of metal (aluminum)–matrix composite (MMC), the liquid-state processing route stands out to be simple, economical, and versatile because aluminum and its alloys usually have a relatively low melting point and low viscosity.[1,2] The liquid-state fabricating route can be divided into the following categories: infiltration, dispersion, spray-casting, and in-situ processing.[1] Among them, the pressure infiltration processing method, also called squeeze casting, has received most of the research and development attention, and has also been successfully applied to produce automobile components by major automakers worldwide, such as Toyota, Honda, and Ford.[3] In this fabricating method, the molten metal matrix (usually aluminum or its alloy) is forced to infiltrate a porous preform, which is made of ceramic reinforcement (fibers or particulate), by applying a pressure difference. The first stage of this manufacturing process is to let the molten metal–matrix completely infiltrate the entire preform, then the second stage is to completely solidify the molten metal in the preform to form the composite. In this paper, however, only the first stage is modeled, and the postinfiltration solidification remains for future research efforts.

There are several physical phenomena involved in the infiltration process, which are very interesting from the standpoint of fluid flow and heat transfer. The first phenomenon is the solidification, which occurs as a result of molten metal–matrix contacting with cooler preform behind the infiltration front; because the superheat of metal–matrix is usually small, the solidification takes place simultaneously with the infiltration. The ceramic porous preform is intentionally kept at a lower temperature than the liquidus temperature of metal–matrix to minimize the chemical interaction between the ceramic material and the metal–matrix.[4] If the molten metal–matrix is an alloy, the solidification will cause nonuniform solute distribution along the infiltration path by either rejecting or incorporating the solute element. The second phenomenon is remelting, which refers to the process where the inlet superheated metal–matrix melts some of the previously solidified matrix. The solidification and remelting will change the preform permeability substantially, and thus change the infiltration flow

dynamics. Infiltration flow, heat, and mass transfer are strongly coupled in the infiltration process of metal–matrix composite production.

Literature survey shows that most of the previous research work in this area are experimental works conducted by material scientists and engineers. The focus of those research works is mainly on the microstructure development and the interfacial chemical interactions. The theoretical analysis of the flow and heat transfer phenomena are presented by only a few investigators. For the infiltration by a pure metal, Mortensen et al.[5] presented a general theory for the infiltration and phase change heat transfer. They also presented a similarity solution for the case of unidirectional, adiabatic infiltration by means of the Boltzmann transformation. Masur et al.[6] experimentally measured the infiltration characterization of pure aluminum, and showed that the experimental results agree well with theoretical predictions. Tong and Khan[7] presented the two-dimensional numerical simulation results for a pure metal. Their results include the evolution of infiltration and remelting fronts, the relationship between total infiltration time, remelting region size, and the operating conditions: pressure difference, preform and inlet metal-matrix temperatures, preform porosity, etc. For the case of alloy, Mortensen and Michaud[8] presented a general theoretical description of infiltration flow, heat transfer, and mass transfer. For the one-dimensional case, they also presented a similarity solution by assuming that the infiltration length is proportional to the square root of time to decouple infiltration flow with heat transfer and mass transfer. Michaud and Mortensen[9] presented some experimental results for the one-dimensional infiltration by Al-4.5 wt% Cu alloy. The solute profile in the composite shows good agreement with theoretical predictions.

Although the one-dimensional infiltration by a hypoeutectic alloy has been studied previously,[8,9] this problem is researched in the present study because of the following reasons.

1) To get a similarity solution, Mortensen and Michaud[8] employed the Boltzmann transformation, which can only be applied to one-dimensional problems. In this paper we try to present a complete numerical formulation of the problem and identify the dimensionless groups that govern the infiltration.

2) The transient behavior of infiltration and the effect of variable porosity (or permeability) can be investigated through the present formulation, we have partially explored these effects in this paper. In the following sections, the model formation is derived from the fundamental conservation laws, then the immobilizing transformation is employed to transform the governing equations into a new set of equations in the computational space. The numerical implementation is given in detail and numerical convergence tests are conducted. Numerical predictions are compared with the experimental measurements and theoretical solutions. The transient behavior of infiltration process, i.e., the evolution of temperature and solute distribution, is presented. The macrosegregation caused by solidification in the composite is investigated through changing operational variables, such as initial preform temperature, inlet superheat of metal–matrix, and the pressure difference. Finally, some conclusions are drawn.

Model Formulation

The physical domain is schematically shown in Fig. 1. It consists of a uniform preform with ς and K_0. At $t = 0$, the molten alloy (Al-4.5 wt% Cu for the present study) at P_1, T_1, and C_0, is driven to infiltrate the porous preform by a pressure difference $P_1 - P_0$. As T_p is usually kept well below alloy liquidus, the heat transfer between the molten alloy and the cooler preform takes place simultaneously with infiltration flow. This results in the partial solidification of the molten alloy, at the same time the inlet superheat of the metal will melt some of the previously solidified matrix. Thus, three different regions exist: 1) the remelting, 2) solidification, and 3) uninfiltrated regions. The solidification process will change not only the preform permeability, but also the solute (Cu) distribution in the composite. For the binary alloy of Al-4.5 wt% Cu, the solute concentration will be enriched downstream of the infiltration path, which has been observed experimentally by Michaud and Mortensen.[9] A similar macrosegregation behavior was also observed by Clyne and Mason[10] for the binary alloy of Al-2.5 wt% Mg.

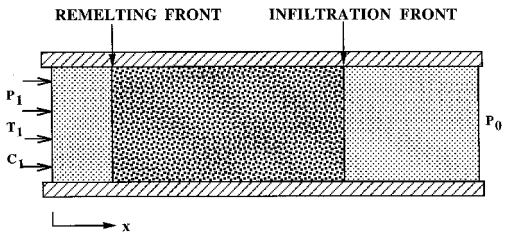

Fig. 1 Schematic of unidirectional infiltration processing of metal–matrix composite.

For the unidirectional infiltration process, flow and heat transfer (including solidification and remelting) can be described by the following equations: continuity, Darcy's law, energy conservation, and solute conservation. The following assumptions are employed to simplify the problem: 1) the infiltration and remelting fronts are one-dimensional planar; 2) heat loss and pressure drop ahead of infiltration front are negligibly small; 3) the gravity effect on the infiltration process is relatively small compared to the pressure difference; 4) local thermal equilibrium; 5) the solute concentration and local temperature are related by the lever rule[11]; 6) the liquidus line of phase diagram is straight; and 7) constant physical properties, the density variation during solidification, or remelting is neglected.

For remelting and solidification regions, the governing equations can be written as follows:

$$\frac{\partial u}{\partial x} = 0 \tag{1}$$

$$u = -\frac{K}{\mu}\frac{\partial p}{\partial x} \tag{2}$$

$$(\rho c_p)_m \left(\sigma \frac{\partial T}{\partial t} + u \frac{\partial T}{\partial x}\right) = \frac{\partial}{\partial x}\left(k_c \frac{\partial T}{\partial x}\right) + \varsigma \Delta h \frac{\partial g_s}{\partial t} \tag{3}$$

$$\frac{\partial C_{\text{av}}}{\partial t} + \frac{u}{\varsigma}\frac{\partial C_l}{\partial x} = 0 \tag{4}$$

where K is $K = K_0$ in the remelting region, but $K < K_0$ in the solidification region, g_s is $g_s \equiv g_s(x)$, $g_s = 0$ in the remelting region; k_c is evaluated by the so-called parallel conduction model,[12] $k_c \equiv \varsigma k_m + (1 - \varsigma)k_p$; and the parameter $\sigma \equiv \varsigma + (1 - \varsigma)\lambda$, $\lambda \equiv (\rho c_p)_p/(\rho c_p)_m$. C_{av} is related to the liquid concentration C_l, solid volume fraction g_s, and the partition coefficient k_p by the lever rule and thermodynamic relation[11]:

$$C_{\text{av}} = [1 - (1 - k_p)g_s]C_l \tag{5}$$

$$T - T_m = m_l C_l \tag{6}$$

where $k_p = 0.171$ for Al–Cu alloy, $m_l = -3.36$ K/wt% Cu. T_m is the melting temperature of solvent (Al in Al–Cu alloy, 933 K). C_0 corresponds to T_0, for example, $T_0 = 918$ K for $C_0 = 4.5$ wt% Cu. If T_1 is higher than T_0, then the inlet molten metal is superheated.

The treatment of preform permeability is an important part of mathematical modeling of the infiltration process. Within the solidification region, the permeability is not a constant, it is position dependent and smaller than the initial preform per-

meability K_0, caused by solidification. For the sake of generality, i.e., not assuming any specific arrangement of fibers, and not invoking any specific permeability calculation model, we adopt the approach employed by Mortensen and Michaud.[8] They assumed that the infiltration length is proportional to the square root of time, which is exactly equivalent to introducing an average permeability K_{av} to simplify the infiltration flow analysis. The average permeability is, basically, an integral average of permeability in the infiltrated (saturated) portion.

Governing Eqs. (1–4) can be nondimensionalized by introducing the following dimensionless variables:

$$U = \frac{uL}{v}, \qquad X = \frac{x}{L}, \qquad \Psi = \frac{K_{av}(P - P_0)}{\mu v}$$
$$\theta = \frac{T - T_p}{T_0 - T_p}, \qquad \bar{C}_{av} = \frac{C_{av}}{C_0}, \qquad \bar{C}_l = \frac{C_l}{C_0} \tag{7}$$

$$\tau = \frac{vt}{L^2}, \qquad Pr_c = \frac{(\rho c_p)_m \nu}{k_c}, \qquad Ste = \frac{(\rho c_p)_m (T_m - T_0)}{\Delta h} \tag{8}$$

The governing equations become

$$\frac{\partial U}{\partial X} = 0 \tag{9}$$

$$U = -\frac{\partial \Psi}{\partial X} \tag{10}$$

$$\sigma \frac{\partial \theta}{\partial \tau} + U \frac{\partial \theta}{\partial X} = \frac{\partial}{\partial X}\left(\frac{1}{Pr_c}\frac{\partial \theta}{\partial X}\right) + \frac{\varsigma}{Ste}\frac{\partial g_s}{\partial \tau} \tag{11}$$

$$\frac{\partial \bar{C}_{av}}{\partial \tau} + \frac{U}{\varsigma}\frac{\partial \bar{C}_l}{\partial X} = 0 \tag{12}$$

The remelting front movement is governed by the interface energy balance

$$-\left.\frac{\partial \theta}{\partial X}\right|_{X=M^-} + \left.\frac{\partial \theta}{\partial X}\right|_{X=M^+} = \varsigma g_s(M^+)\frac{Pr_c}{Ste}\frac{\partial M}{\partial \tau} \tag{13}$$

where $X = M$ refers to the remelting front position, which is a function of time. The boundary conditions are as follows: at the inlet gate: $C_1 = C_0$, $\Psi = \Delta\Psi$, $\theta = \theta_1$; at the infiltration front: $\Psi = 0$; and at the remelting front: $\theta = 1$. The other boundary conditions at the infiltration front are no heat or mass transferred out of the infiltration front. Numerical implementation will be given in the next section. Observing the governing equations and the boundary conditions, we can identify the following dimensionless groups that determine the infiltration and phase change heat transfer process: dimensionless pressure difference $\Delta\Psi$, inlet temperature θ_1, porosity ς, Stefan number Ste, and Prandtl number Pr_c. The present problem is a typical moving boundary problem, two fronts (infiltration and remelting) are time dependent. The well-known Landau transformation is employed to map the two time-dependent regions into two fixed unit regions. After transformation, Eqs. (11) and (12) take the following forms in the new space:

$$\frac{\partial(\sigma J\theta)}{\partial \tau} + \frac{\partial}{\partial \xi}\left[(U - \sigma X_\tau)\theta - \frac{1}{JPr_c}\frac{\partial \theta}{\partial \xi}\right] = \frac{\varsigma}{Ste}\left(J\frac{\partial g_s}{\partial \tau} - X_\tau \frac{\partial g_s}{\partial \xi}\right) \tag{14}$$

$$\frac{\partial(J\bar{C}_{av})}{\partial \tau} + \frac{\partial}{\partial \xi}(-X_\tau \bar{C}_{av}) = -\frac{\partial}{\partial \xi}\left(\frac{U}{\varsigma}\bar{C}_l\right) \tag{15}$$

where X_τ is the pseudovelocity associated with immobilization of moving fronts.[13] Through Eqs. (5) and (6), Eqs. (14) and (15) are coupled in the solidification region. While in the remelting region, only Eq. (14) needs to be solved with the volume fraction of solidification g_s approaching zero.

Table 1 Grids refinement test results

Grids	51	61	71	81
Temperature	0.804236	0.803666	0.803234	0.802884
Concentration	4.055126	4.114150	4.158400	4.192695

Numerical Procedure

Equations (14) and (15) are discretized by the control-volume-based finite difference method.[14] The power-law scheme is used for the convection–diffusion terms in Eq. (14). The upwind scheme[14] is used for convection term in Eq. (15). To initiate the numerical simulation, a very small (0.04) region near the inlet gate is selected to be the initial infiltrated region, of which an even smaller region (0.002) is selected to be the initial remelting region. The numerical tests show that these selections have a negligible effect on the final temperature, solid volume fraction and solute concentration profiles. Once the initial regions are determined, by assuming the initial temperature profile to be linear, the initial temperature and solid volume fraction distribution can be determined by the energy and mass conservation, i.e., the energy and solute mass carried in by molten metal equal to the energy and solute mass existing in that initial region.

The treatments of infiltration front boundary conditions for heat and mass transport equations are worth mentioning here. For the heat transfer Eq. (14), although we assume that there is no heat loss ahead of the infiltration front, there is a convection term that carries cooler fiber into the control volume across the infiltration front after immobilization of infiltration front. For mass transfer Eq. (15), no mass is transferred in or out of the infiltration front. Because the solidified metal matrix remains where it forms, and the average solute concentration is strongly dependent upon the volume fraction of solidification, the real convection term, i.e., convection term in physical space, is treated explicitly as a source term in Eq. (15). The numerical results show the present treatment produce physically reliable results. The total energy and solute concentration conservation calculation, i.e., comparing the energy and concentration integral along the infiltrated composite to the energy and solute carried in by molten metal matrix, showed that the relative errors are within 0.5 and 3% for energy and solute conservation, respectively.

The time step is selected such that the infiltration front jumps 0.0005 per time step. The movement of the remelting front is then determined by interface energy Eq. (13). The numerical tests show that the time step is small enough to guarantee the convergence of numerical results to within 0.1%. The grids' independence is desired for any numerical simulation. Different grid sizes have been tested to reach a compromise between numerical accuracy and computational cost. Because the solidification region is a primary concern for the present problem, the grids' refinement tests have been done on the solidification region. Table 1 shows a comparison of results for $\Delta\Psi = 166$, which corresponds to the sample no. 1 in the previously mentioned experimental investigation,[9] porosity $\varsigma = 0.757$. The temperature and solute concentration in Table 1 refer to the physical quantities at the infiltration front after infiltration stops. Based on the test results, we see that 71 grids can produce about 1% accuracy of solid concentration and temperature. For the remelting region, we used 21 grids, because that region is usually much smaller than the solidification region.

Results and Discussion

Table 2 lists the physical properties of aluminum and SAFFIL®. All of the numerical results reported in this paper are

Table 2 Physical properties of pure aluminum and SAFFIL[a]

	ρ, kg/m^3	C_p, J/kg·K	μ, Pa·s	k, W/m·K	T_m, K	Δh, kJ/kg
Al(1)	2400	1083	1.3×10^{-3}	93	933	398
SAFFIL	3300	1213	——	8	——	——

[a]SAFFIL is the trademark of ICI Americas Inc., Wilmington, Delaware; nominally 3-μm diam delta-alumina.

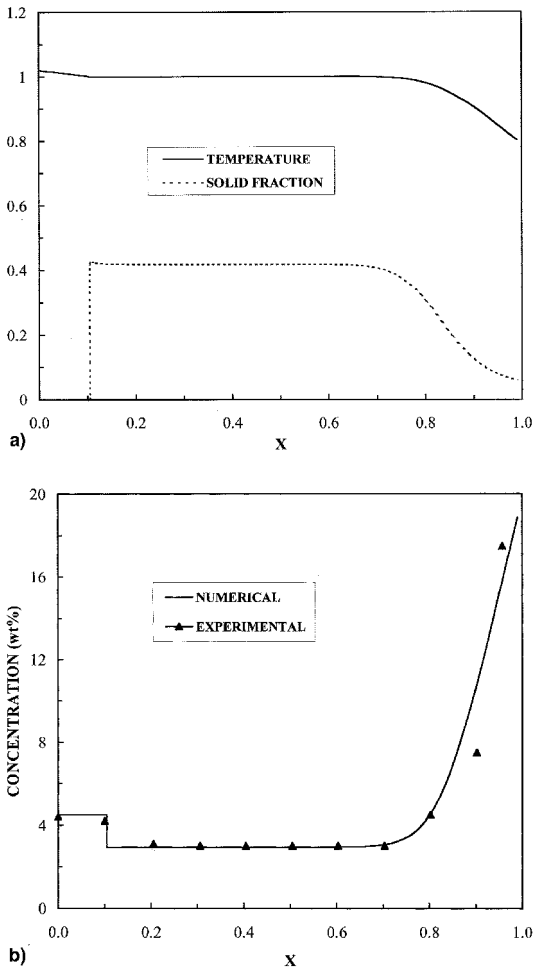

Fig. 2 a) Temperature and solid fraction distribution, and b) average solute distribution (DC = 166, u_1 = 1.019, w = 0.757, and *Ste* = 0.7075).

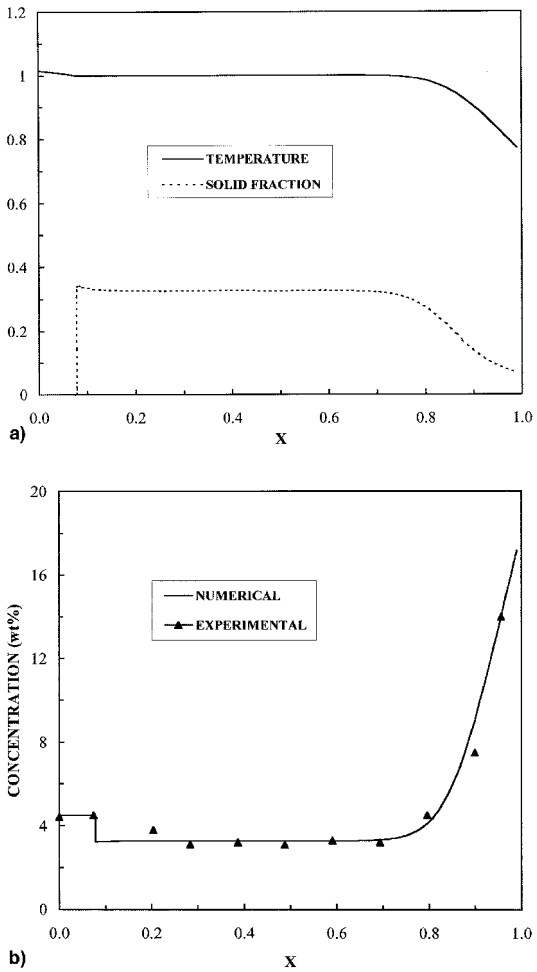

Fig. 3 a) Temperature and solid fraction distribution, and b) average solute distribution (DC = 239, u_1 = 1.015, w = 0.755, and *Ste* = 0.5442).

based on these properties. In this section, we try to present a comprehensive picture of the involved physical processes (infiltration, solidification, and remelting), at the same time, we make some comparison with the experimental results[9] and the theoretical predictions[8] whenever possible.

Michaud and Mortensen[9] carried out a series of experimental investigations of the infiltration of Al-4.5 wt% Cu alloy. Because the temperature and solidification volume fraction distribution are difficult to measure in the infiltrated preform after infiltration, Michaud and Mortensen[9] experimentally measured only the solute (copper) concentration in the composites. To simulate the infiltration process and compare their experimental results,[9] we chose the same parameters as those of the experimental work. The following equation relates $\Delta\Psi$ to the parameter ψ (m/$\sqrt{}$s) used by Mortensen and Michaud,[8,9]

$$\Delta\Psi = s\psi^2/2v \tag{16}$$

Figures 2–4 present the solute concentration, temperature, and solidification volume fraction profiles for three different dimensionless pressure differences $\Delta\Psi$ = 166, 239, and 45, these pressure differences represent the experimental conditions of samples no. 1, 5, and 2, i.e., ψ = 0.0154, 0.0185 and 0.008 m/$\sqrt{}$s, respectively. Thermal conditions for these samples are T_1 = 923 K and T_p = 658 K, T_1 = 921 K and T_p = 718 K, T_1 = 923 K, and T_p = 623 K, respectively. They can be transferred into dimensionless thermal boundary conditions by means of Eq. (7). Generally, the numerical results agree very well with the experimental measurements of the solute concentration profile. The copper concentration jumps down from the initial concentration at the remelting front, and then remains almost unchanged until the final part of the composite, where the solute concentration is highly enriched as a result of solidification.

Comparing these Figs. 2–4, we also observe the effect of dimensionless pressure difference on the macrosegregation patterns, as well as the temperature profiles. When $\Delta\Psi$ is reduced from 166 (Fig. 2) to 45 (Fig. 4), the macrosegregation of solute becomes less severe, i.e., the copper concentration at infiltration front decreases from about 20 to 14%. The temperature profile also becomes flatter, i.e., the dimensionless temperature at infiltration tip increases from 0.8 to 0.9. But

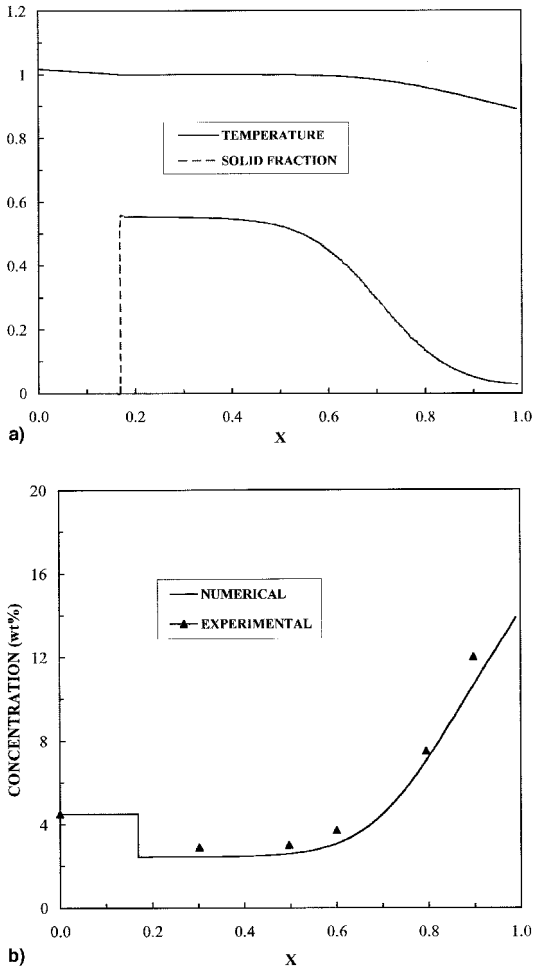

Fig. 4 a) Temperature and solid fraction distribution, and b) average solute distribution (DC = **45,** u_1 = **1.017,** w = **0.754, and** *Ste* = **0.8027).**

when $\Delta\Psi$ is increased from 166 to 239 (Fig. 4), the macrosegregation pattern changes very little, because the initial preform temperature for Fig. 3 (718 K) is higher than that for Fig. 2 (623 K). The lower the initial fibrous preform temperature, the more severe the macrosegregation will be, this is as expected.

The selection of pressure level is very important for the practical fabrication of metal–matrix composites. For the case of binary alloy, it will be determined not only for the compromise between the production speed and the capital cost of equipment, but also for the macrosegregation, because the lower pressure level is favorable to reduce macrosegregation of solute element.

The heat transfer feature in the remelting region can also be observed from the temperature profiles of all three cases; the heat transfer mechanism is dominated by conduction rather than by convection because all temperature profiles are nearly straight lines. This phenomenon can be attributed to the fact that the remelting region is small, and the infiltration velocity is relatively small, while the thermal conductivity of the metal–matrix is large.

Figure 5 shows the evolution of temperature, copper concentration, and solid volume fraction profiles for a representative case ($\Delta\Psi$ = 166, θ_1 = 1.019, ς = 0.757, and *Ste* = 0.7075), which corresponds to sample no. 1 studied by Michaud and Mortensen.[9] Five different time instants, τ = 7.85E−5, 3.43E−4, 7.894 × 10^{-4}, 1.42E−3, and 2.27E−3, are chosen to show the evolution process. The numerical results show that infiltration flow, heat, and mass transfer do display similar features. In other words, the temperature and

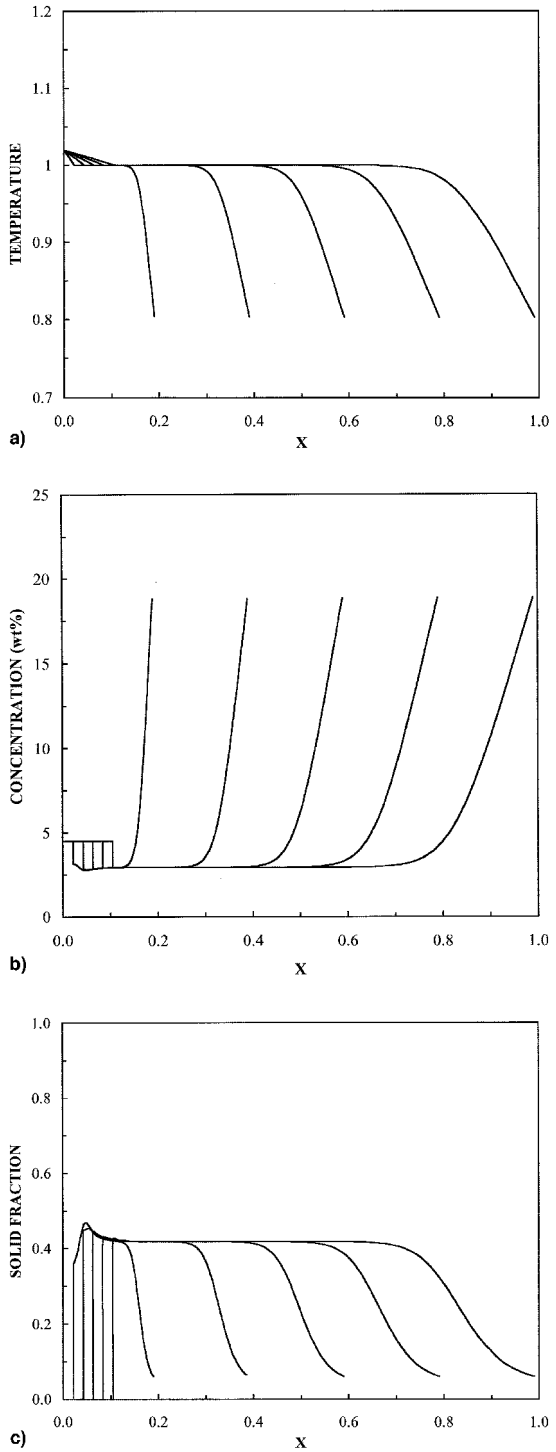

Fig. 5 a) Evolution of temperature, b) solid volume fraction, and c) average solute concentration (DC = **166,** u_1 = **1.019,** w = **0.757, and** *Ste* = **0.7075).**

concentration profiles are very similar for all of the time instants. The temperature and copper concentration at the infiltration tip are almost the same. But the volume fraction of solid does show some difference among these five different instants. As mentioned in a previous section, the solid volume fraction at the infiltration front is determined by matching the temperature and the concentration at the infiltration tip, i.e., lever rule, see Eq. (5).

Figure 6 shows the comparison between the present numerical solution and the theoretical (similarity) solution given by Mortensen and Michaud[8] for the case of dimensionless pres-

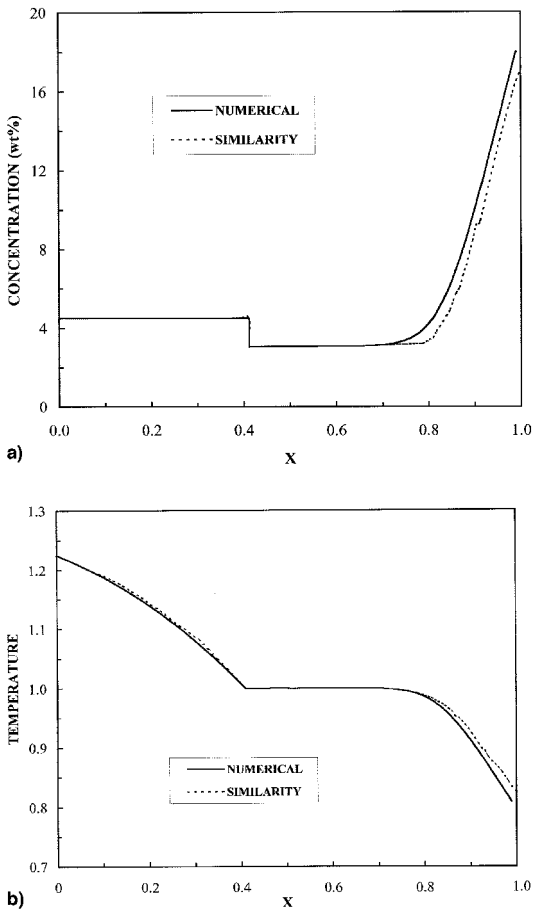

Fig. 6 Comparison between present numerical solution and the similarity solution (DC = **166,** u_1 = **1.2245,** w = **0.76, and** *Ste* = **0.6667).**

sure difference $\Delta\Psi$ = 166 (ψ = 0.015 m/$\sqrt{s}$), inlet metal–matrix temperature T_1 = 973 K, and initial preform temperature T_p = 673 K. Because the inlet metal–matrix state is highly superheated, the remelting region is much larger than that in the previous cases. The temperature profile in the remelting region demonstrates the convection effect, i.e., deviate from the straight line. The first part in the solidification portion is featured by the constant temperature and concentration, while the second part is featured by the sharp temperature gradient and severe solute segregation. Overall, the numerical results agree well with the similarity solution for the most part of the infiltrated composites. The discrepancy occurs at a small region near the infiltration front, where the numerical results give lower tip temperature and higher tip solute concentration. The reason for the difference may be attributed to the different tip boundary condition used in this paper from that used by Mortensen and Michaud.[8,9]

The total infiltration time is defined as the time interval required from the beginning of infiltration to the end of infiltration. According to the present nomenclature, the total infiltration time can be correlated by the following equation:

$$\tau_{\text{TOTAL}} = \varsigma/2\Delta\Psi \tag{17}$$

This equation can be derived from Eq. (16). The practical implication of Eq. (17) is that since the total infiltration time, the applied pressure difference can be very accurately measured in experiments of the infiltration processing of metal–matrix composites, the dimensionless pressure difference $\Delta\Psi$ can be thus determined from Eq. (17), so can the average permeability of preform K_{av} [see Eq. (7)]. K_{av} is generally a strong function of the volume fraction of solidification which, as shown in this section, demonstrates a similarity feature during unidirectional infiltration process, Therefore, Eq. (17) provides a means of estimating the dimensionless pressure difference $\Delta\Psi$. Once the dimensionless pressure difference is known, the average solute distribution and the volume fraction of solid can be easily calculated from either the numerical simulation or the similarity solution. Because the infiltration time is an important parameter for engineering design, Eq. (17) provides a useful correlation relating the infiltration time to the preform porosity and pressure difference.

Conclusions

A numerical formulation of unidirectional adiabatic infiltration, heat, and mass transport in a porous preform has been presented in this paper. The model derivation is based on the basic conservation laws. The model equations are nondimensionalized for generality, and the dimensionless parameters are identified to govern the pressure infiltration. The numerical algorithm for solving the model equations are presented in detail. Two moving boundaries are immobilized by the Landau transformation. The numerical predictions of average solute concentration distribution in the composites agree well with the experimental measurements. Comparison with the similarity solution has been made to check the difference between the present work and the theoretical work because of the different boundary conditions used. The numerical results agree well with the theoretical results, except for a small region near the infiltration tip. Based on the present numerical work, the following conclusions can be reached:

1) The governing parameters for pressure infiltration are identified as $\Delta\Psi$, θ_1, *Ste*, and ς.

2) The numerical results show that the infiltration, heat transfer, and mass transfer do display similarity features during the pressure infiltration process after a certain length of infiltration, as shown in Fig. 5.

3) Severe macrosegregation patterns exist near the infiltration tip. It is also observed that lower pressure difference and higher preform temperature will help alleviate the macrosegregation in the cast composite.

4) The total infiltration time has been correlated [Eq. (17)], this equation can be employed to detect the solidification behavior during the unidirectional adiabatic infiltration process.

References

[1]Mortensen, A., Cornie, J. A., and Flemings, M. C., "Solidification Processing of Metal-Matrix Composites," *Journal of Metals*, Feb. 1988, pp. 12–19.

[2]Rohatgi, P., and Asthana, R., "The Solidification of Metal-Matrix Particulate Composites," *Journal of Metals*, May 1991, pp. 35–41.

[3]Mortensen, A., and Koczak, M. J., "The Status of Metal-Matrix Composite Research and Development in Japan," *Journal of Metals*, March 1993, pp. 10–18.

[4]Fukunaga, H., and Goda, K., "Formation and the Role of the Solidified Layer on a Fiber During the Fabrication of Fiber Reinforced Metal by the Liquid Process," *Journal of Japanese Institute of Metals,* Vol. 49, 1985, pp. 78–83.

[5]Mortensen, A., Masur, L. J., Cornie, J. A., and Flemings, M. C., "Infiltration of Fibrous Preform by a Pure Metal: Part I. Theory," *Metallurgical and Materials Transactions A*, Vol. 20A, No. 11, 1989, pp. 2535–2547.

[6]Masur, L. J., Mortensen, A., Cornie, J. A., and Flemings, M. C., "Infiltration of Fibrous Preform by a Pure Metal: Part II. Experiment," *Metallurgical and Materials Transactions A*, Vol. 20A, No. 11, 1989, pp. 2549–2557.

[7]Tong, X., and Khan, J. A., "Infiltration and Solidification/Remelting of a Pure Metal in a Two Dimensional Porous Preform," *Journal of Heat Transfer*, Vol. 118, No. 1, 1996, pp. 173–180.

[8]Mortensen, A., and Michaud, V., "Infiltration of Fibrous Preform by a Binary Alloy: Part I. Theory," *Metallurgical and Materials Transactions A*, Vol. 21A, No. 7, 1990, pp. 2059–2072.

[9]Michaud, V., and Mortensen, A., "Infiltration of Fibrous Preform by a Binary Alloy: Part II. Further Theory and Experiment," *Metallurgical and Materials Transactions A*, Vol. 23A, No. 8, 1992, pp. 2263–2280.

[10]Clyne, T. W., and Mason, J. F., "The Squeeze Infiltration Process for Fabrication of Metal-Matrix Composites," *Metallurgical and Materials Transactions A*, Vol. 18A, No. 6, 1987, pp. 1519–1530.

[11]Kurz, W., and Fisher, D. J., *Fundamentals of Solidification*, 3rd ed., Trans Tech Publications, Aedermannsdorf, Switzerland, 1992, pp. 117–130.

[12]Nield, D. A., and Bejan, A., *Convection in Porous Medium*, Spring–Verlag, New York, 1992, Chaps. 1–4.

[13]Kim, C. J., and Kaviany, M., "A Numerical Method for Phase Change Problems," *International Journal of Heat and Mass Transfer*, Vol. 33, No. 12, 1990, pp. 2721–2734.

[14]Patankar, S. V., *Numerical Heat Transfer and Fluid Flow*, Hemisphere, Washington, DC, 1980, Chaps. 2–5.